

# INVESTIGATION OF THE BULK DRAG COEFFICIENT OF NATURE-BASED BREAKWATER BY FLOW EXPERIMENTS

Ngo Thi Thuy Anh<sup>a</sup>, Dao Hoang Tung<sup>b,\*</sup>, Mai Cao Tri<sup>c</sup>, Nguyen Hong Lan<sup>b</sup>

<sup>a</sup>*Faculty of Civil Engineering, Thuyloi University, 175 Tay Son road, Kim Lien ward, Hanoi, Vietnam*

<sup>b</sup>*Faculty of Marine Science and Island, Hanoi University of Natural Resources and Environment, 41A Phu Dien road, Phu Dien ward, Hanoi, Vietnam*

<sup>c</sup>*Faculty of Coastal and Offshore Engineering, Hanoi University of Civil Engineering, 55 Giai Phong road, Bach Mai ward, Hanoi, Vietnam*

## Article history:

Received 10/9/2025, Revised 16/10/2025, Accepted 30/10/2025

---

## Abstract

Nature-based solutions for nurturing the coast, particularly mud and mangrove coasts, have gained significant attention and are emerging as a new trend in the context of coastal engineering. In this study, the bulk drag coefficients of a permeable structure, a brushwood fence, are investigated and assessed by Darcy-Forchheimer flow experiments. Two samples, assembled from a number of bamboo cylinders with two different densities (607 and 1209 cylinders/m<sup>2</sup>) and an average diameter of 0.02 m, are installed inside a square tube (26 cm × 26 cm). A steady flow discharge is forced through the samples, which naturally creates a hydraulic loss (a difference in water levels) between the upstream and downstream sides. The forces created by hydraulic gradient, a ratio of hydraulic loss to sample widths, are then investigated as the drag forces, in which the bulk drag coefficients ( $\bar{C}_d$ ) plays a vital role in this study. The findings from this investigation conclude that the bulk drag coefficients depend on the flow stages (represented by Reynolds number,  $Re$ ) and reach significantly high values at low  $Re$  but become stable at high  $Re$ . Our findings of  $\bar{C}_d$  indicate to have a similar trend to previous studies, that is, 2.0 for  $Re > 2000$  (turbulent flow) for cases with a lower density of 607 cylinders/m<sup>2</sup>, while  $\bar{C}_d$  is greater than 2.0 for  $Re < 2000$  (laminar flow).

**Keywords:** brushwood fence; bulk drag coefficients; Darcy-Forchheimer; Mekong Delta; mangroves.

[https://doi.org/10.31814/stce.huce2025-19\(4\)-06](https://doi.org/10.31814/stce.huce2025-19(4)-06) © 2025 Hanoi University of Civil Engineering (HUCE)

---

## 1. Introduction

Nature-based solutions have become a new trend in coastal protection, as the assessment of grey structures has concluded that they cause more harm than good to the coastal area. Along mud and mangrove coasts, e.g. Mekong Delta, wooden barriers (so-called wooden fences in several particular coasts) have brought a certain benefit for the coasts, especially for mangrove or mud coasts [1–3]. This solution is also easy to access due to its convenient from lower cost, and technique.

It is recognised that the nature-based solutions can also be a combination of hard/grey structures with natural ecosystems and nature-based structures, for example, mangroves and porous breakwater [4], wooden fences and mangroves in front of sea dikes [5]. In most of the porous structures supporting mangroves at the frontline, a similar structure, including a frame and permeable parts, is recognisable (Fig. 1), and plays a vital role in reducing wave and wave-induced flow before it reaches the mangroves. Furthermore, the primary source of that reduction is the resistance of the part inside the frame, commonly referred to as the inner parts, as previously concluded in studies [4–14].

The resistance of the porous parts, including the branches as in the bamboo fence or pile-rocks as in the permeable breakwater (Fig. 1), is mainly received from the drag forces from flow velocity

---

\*Corresponding author. E-mail address: [dhtung@hunre.edu.vn](mailto:dhtung@hunre.edu.vn) (Tung, D. H.)



(a) Pile-rock breakwater



(b) Bamboo fence

Figure 1. Porous structure, (a) Pile-rock breakwater (2024) and (b) Bamboo fences (2016), in the Mekong Delta coast. Photo courtesy of Dao Hoang Tung

along the structure's width. In general, the drag force on the surface of any cylinders (for brushwood fences) and pile-rocks (for permeable structures) is used to achieve quantitative wave flow. Then, the drag coefficient, both theoretically and empirically, expresses the resistance of these similar media. A common procedure for quantifying the drag coefficient is to employ the Morison equation for drag force on circular cylinders [15–18] and pile-rocks in breakwaters or dikes [19, 20].

In particular, the drag force driven by the complex flow, including both laminar and turbulent conditions, is strongly dependent on the bulk drag coefficient, which is represented for the entire porous medium. It is noted that the aggregate of cylinders with irregular diameters, as seen in the inner part of the bamboo fence (Fig. 1(b)), and similar to the combination of different pile-rock diameters found in porous breakwater (Fig. 1(a)). Therefore, a feasible way of representing the drag force is an adaptation from the concept of the volume average [21–23]. As a result, the force of the permeable medium in the form of hydraulic gradient can be obtained by the hydraulic gradient induced from Darcy [23] for viscous flow and Forchheimer [21] for both viscous and turbulent flow. However, each flow state can be affected differently due to the differences in hydraulic gradients resulting from the friction terms of the porous medium [24–27].

Globally, the Darcy–Forchheimer equation has been commonly used to obtain the drag force in a porous medium formed by granular material, e.g., gravel, coarse sand, or fine sand [24, 25] and even for permeable beds of spherical particles [20–23], packed column with granular materials [26], and porous rock structures [27, 28]. In an application for the inner parts of the wooden fence or the permeable breakwater, their characteristics, including the random structures and different diameters, create a medium that makes it almost impossible to obtain the drag coefficient just by measuring a single element of the structure's body. As a result, the Darcy–Forchheimer method is a more practical approach for obtaining the bulk drag coefficient.

In this study, the hydraulic gradient obtained from Darcy–Forchheimer experiments will be derived as a pre-assessment for the bulk drag force, as represented by the Morison equation. The relation of the bulk drag coefficient and flow velocity, represented by the Reynolds Number, will also be achieved from Darcy–Forchheimer experiments. In the following section, the methodology will carry out the Morison equation and the Darcy–Forchheimer approach for drag force and its relation to the bulk drag coefficient. A series of flow tests will be presented to provide a close view of the

hydraulic gradient. Finally, the results and conclusion will be presented.

## 2. Methodology

In this study, the Darcy and Forchheimer equations are applied in a steady flow experiment to determine the hydraulic gradient of the permeable medium, specifically the brushwood sample. This gradient is a result of the flow forces acting in front of each bamboo cylinder and their respective forms, including the arrangement and gaps between cylinders. In this section, brief flow experiments will be carried out in conjunction with the Darcy-Forchheimer equations to obtain the hydraulic gradients. As a result, the drag force and the bulk drag will be achieved.

### 2.1. Drag force of a permeable medium

The drag force formula for an array of cylinders, presenting for the inner parts of the brushwood, can be derived as follows:

$$F_D = \frac{1}{2} \rho D N \bar{C}_d u^2 \quad (1)$$

where  $\rho$  (kg/m<sup>3</sup>) is the water density,  $D$  (m) is the cylinder diameter,  $N$  (cylinders/m<sup>2</sup>) is the number of cylinders in an area, and  $u$  (m/s) is the flow velocity.

The bulk drag coefficient ( $\bar{C}_d$ ) is a dimensionless parameter that illustrates the relationship between the quality of flow reduction over a permeable medium. In this study, the  $\bar{C}_d$  is presented for the inner parts of the bamboo fences (Fig. 1(b)) and is strongly related to flow velocity. However, it is challenging to measure the flow inside a complex structure, similarly to a bamboo fence (Fig. 1(b)). Consequently, the  $\bar{C}_d$  will be connected to the Reynolds number ( $Re = \frac{uD}{\nu}$ , with  $\nu$  (m<sup>2</sup>/s) is the kinematic viscosity), which describes the flow stage in exchange. The  $\bar{C}_d$  relatively depends on the quantified number of  $Re$  that previous studies have carried out. At the laminar flow stage over cylinders ( $Re < 40$ ), the  $\bar{C}_d$  are rapidly increased due to a high drag force generated at a low flow velocity [29]. However, the higher flow velocity ( $Re > 200$ ), the more stable of  $\bar{C}_d$ , relatively equal to 1.0 if there is a single cylinder and 1.5 if there is an array of cylinders [30, 31].

### 2.2. Darcy-Forchheimer equations

The Darcy-Forchheimer equations are presented for the hydraulic pressure under flow stages, the laminar and turbulent flows, over a permeable medium. The hydraulic pressure differences at the upstream and downstream sides of the structure occur during an active current of an incompressible fluid over the structure, such as a brushwood fence. Hence, the hydraulic gradient over the objective width ( $G_B$ ) can be written as:

$$G_B = \frac{1}{g\rho} \Delta P \Delta b \quad (2)$$

where  $\Delta P$  is the pressure difference at the upstream and downstream side of the brushwood fence,  $\Delta b$  is the sample thickness,  $g$  and  $\rho$  are the gravitational acceleration (m<sup>2</sup>/s) and water density (kg/m<sup>3</sup>).

The forces over a porous medium have two components, consisting of the friction and drag forces. It is assumed that the frictional forces can be neglected due to the small effects of materials. As a result, the drag force ( $F_D$ ) consists of laminar and turbulent components, which are presented as pressure forces obtained from the Darcy-Forchheimer equation. The force and its components can be written as:

$$F_D = P_{Lam} \rho u + P_{Tur} \rho u^2 \quad (3)$$

where  $P_{Lam}$  and  $P_{Tur}$  are the pressure components in laminar and turbulent flow states, respectively (it is noted that those components are the dimensionless parameters);  $\rho$  (kg/m<sup>3</sup>) is the water density;

and  $u$  (m/s) is the flow velocity. In Eq. (3) the pressure components,  $P_{Lam}$  and  $P_{Tur}$  are the dependent components on material diameters, porosity and the flow velocity that only apply for steady-state flow (see Darcy [21–23]). It is also noted that the pressure differences will appear with both pressure components during the active flow.

As a result, the hydraulic gradient can be rewritten from Eqs. (1), (2) and (3), and it can be yielded as:

$$G_B = \frac{DN\bar{C}_d u^2}{2g} \quad (4)$$

### 2.3. Hydraulic gradient experiments

The hydraulic gradients were obtained from a series of experiments in the Hydraulic Engineering Laboratory at the Delft University of Technology. The brushwood fences were installed inside a square tube with a cross-sectional dimension of 26 cm. A larger tank with a width of 1.0 m and a height of 2.0 m covered the tube, allowing for reading the water depth difference. A steady flow was then pushed through the fence with a fixed discharge rate  $Q$  (m<sup>3</sup>/s<sup>3</sup>) to achieve the desired difference in water level (see Fig. 2). Two pressure sensors with a range of up to 5 PSI (Pounds per square inch) were installed at the upstream and downstream sides of the fences to measure the water level. A flow discharge moved through the tube (with samples) was kept for a certain time to receive stable and steady water depths and data signals. As a result, the flow velocity over the total area (26 cm × 26 cm) of the tube was yielded as:

$$u_n = \frac{Q}{A.n} \quad (5)$$

where,  $Q$  (m<sup>3</sup>/s) is the flow discharge going through the area  $A$  (m<sup>2</sup>),  $n$  is the porosity of the medium, and the  $u_n$  is the porous velocity considered as the velocity inside the medium [28, 32]. The signal received by the pressure sensors was recorded in voltage with a sampling frequency of 50 Hz (i.e., 50 data signals per second), and then converted to water level (H) using linear regression relations. The hydraulic gradient then can be calculated as:

$$G_B = \frac{\Delta H_{Pr}}{W} \quad (6)$$

where  $\Delta H_{Pr} = |H_1 - H_2|$  is the hydraulic pressure difference over the sample width  $W$  (m). It is noted that the pressure values will exhibit a certain difference at different flow velocities. In Table 1, the uncertainty associated with flow velocities is presented to ensure the accuracy of the devices. It is recognised that only a few millimetres' differences between devices are presented, showing the accuracy of the measurements.

Table 1. The uncertainties between pressure sensors in two different flow velocities

$Q$ (m <sup>3</sup> /s)	$H_{p,1}$ (m)	$H_{p,2}$ (m)
0.00	$8.3 \times 10^{-2} \pm 5.10^{-3}$	$6.9 \times 10^{-2} \pm 4.10^{-3}$
$23.10^{-3}$	$0.68 \pm 8.10^{-2}$	$0.67 \pm 2.10^{-2}$

Brushwood samples were set at different widths, and each was tested at various steady flow discharges, ranging from 0.001 m<sup>3</sup>/s to 0.025 m<sup>3</sup>/s. Samples were examined with several widths ranging from 0.27 m to 0.46 m. The main materials used to set up a sample were bamboo cylinders with a diameter of 0.02 m, kept at the same scale as the real brushwood fence (Fig. 1(b)). As observed from Fig. 1(b), it is assumed that the complex arrangement will lead to a challenge in interpreting



hydraulic mechanisms inside the structures and quantifying the accurate density. Therefore, only one arrangement, a staggered configuration with a fixed density (also the porosity), was applied in this study (Fig. 2). As seen in Fig. 2(b), (c), there were several layers of bamboo cylinders for each width for a test, in which a number of cylinders were up to 8 per layer for the density of 1209 cylinders/m<sup>2</sup> and up to 4 per layer for the density of 607 cylinders/m<sup>2</sup>. Three fence widths were tested for each flow test, starting from 0.27 m for both samples. It is note that the sample should be thick enough. The sample descriptions used in the experiments are described in Table 2.

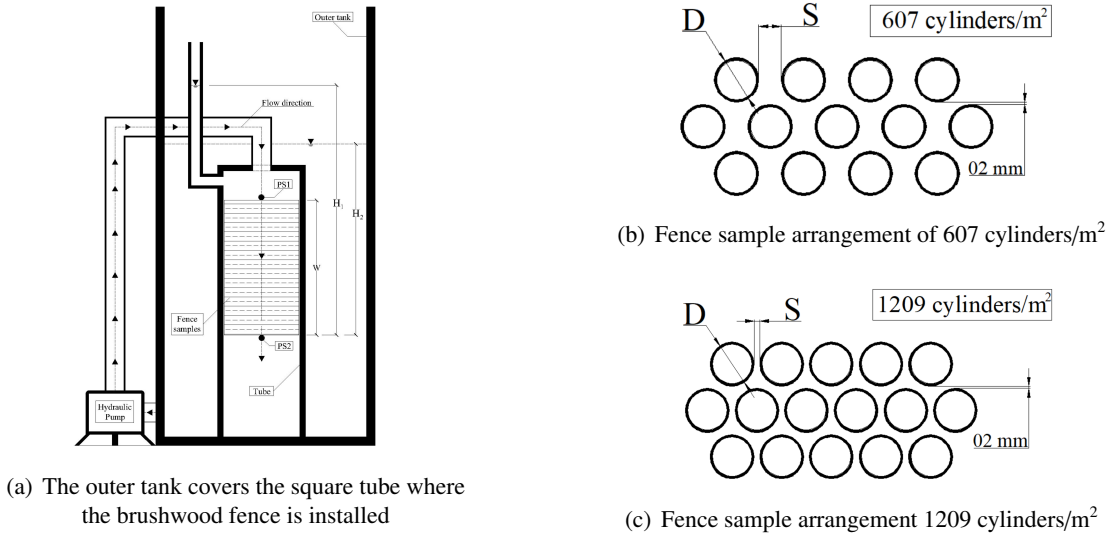




Figure 2. Darcy-Forchheimer experiment settings. (a) Simplified flow experiments, (b) and (c) Bamboo cylinders arrangement for two densities

Table 2. Fence samples used in the flow test

Case	Sample	Width ( $B$ , m)	Density (cylinders/m <sup>2</sup> )	Porosity ( $n$ )	$Q$ (m <sup>3</sup> /s)
Sample 1		0.27	607	0.80	0.005 to 0.025
		0.37			
		0.46			
Sample 2		0.27	1209	0.62	0.005 to 0.025
		0.37			
		0.46			

### 3. Results

In this section, the hydraulic pressure differences are linked together with the porous velocity for further investigation. Then, the relationship between the flow stage parameter, the Reynolds number ( $Re = u_n D / \nu$ ), and the bulk drag coefficient will be presented and explained with the trend equations for both samples.

#### 3.1. Pressure gradient illustration

The hydraulic gradient ( $G_B$ ), known as the hydraulic loss, between the upstream and downstream of the fence is indicated as in Figs. 3 and 4. Here, they are plotted together with porous velocity ( $u_n$ ) to have the links of thicknesses and densities.

In Fig. 3, the hydraulic gradient is illustrated in samples of varying widths, with two densities: 607 cylinders/m<sup>2</sup> and 1209 cylinders/m<sup>2</sup>. As shown in this figure, an increase in flow velocity results in a corresponding increase in hydraulic gradient across a given width. For the first case in Fig. 3(a), the  $G_B$  reaches its maximum value of around 0.3 when the flow reaches its highest value of 0.4 m/s. Meanwhile, the hydraulic gradient reaches a higher value for the case with the higher density of 1209 cylinders/m<sup>2</sup>, at the highest velocity.

It is noted that all  $G_B$  of every width are matched together, even though it is in fact that the thinner thickness results in more flows going through the fence. As shown in Fig. 2, the pressures at the top of the samples are indicated as being less than those at the bottom, leading to relatively different water levels at the surface between two locations. When the flow velocity increases, pressures at the top (entrance of the flow) increase and occur for all tested widths. However, if considering the hydraulic gradient over a width, the water depth differences will be independent of an increase in flow velocity. It is noted that side effects may appear and affect the recorded data. Furthermore, the pressure sensors are installed in the centre of the samples, resulting in pressure only at the centre, rather than at the sides.

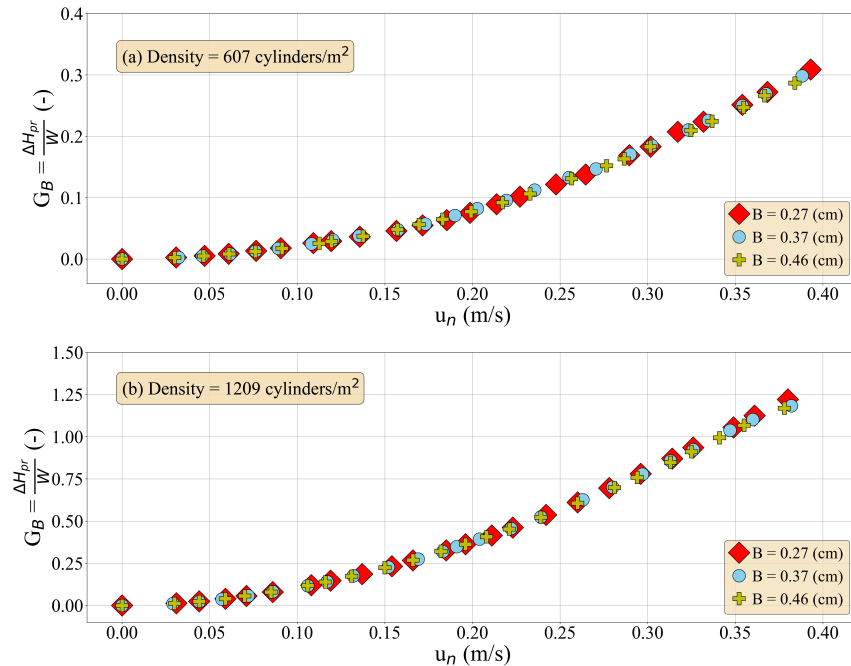


Figure 3. Hydraulic gradient in three tested widths for two different densities, 607 and 1209 cylinders/m<sup>2</sup>

The hydraulic gradients also differ in density, as shown in Fig. 4. The  $G_B$  values increase gradually at flow velocities below 0.1 m/s. However, the higher gaps between two cases are more clear at higher flow velocities, greater than 0.1 m/s. For most cases, water can move relatively easy between cylinders, resulting in the  $G_B$  increasing with flow velocity. However, it is noted that the higher the density, the greater the water block through a sample width. The result in Fig. 4 shows that the  $G_B$  values of the case with 1209 cylinders/m<sup>2</sup> are nearly four times higher than those of the case with about half the density, 607 cylinders/m<sup>2</sup>. This result also indicates that hydraulic gradients are independent of width but significantly depend on density, leading to the next results regarding the bulk drag coefficient.

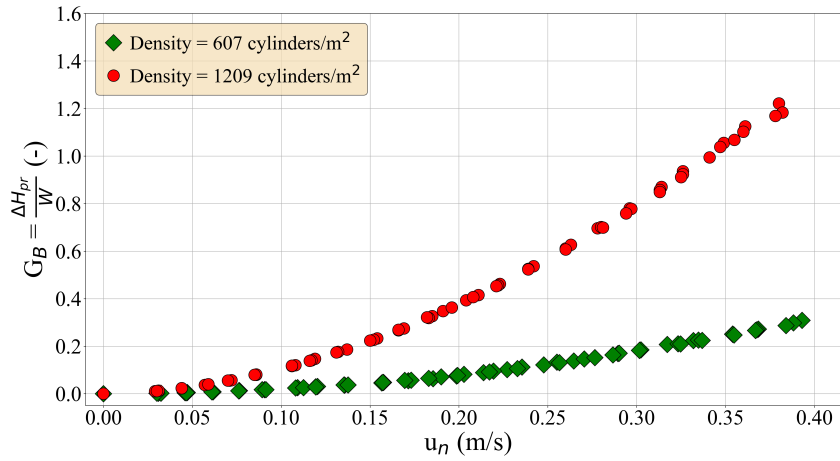


Figure 4. Hydraulic gradient of two cases, 607 and 1209 cylinders/m<sup>2</sup>

### 3.2. Bulk drag coefficient via Reynolds Number

The drag coefficient is a crucial component in the drag forces generated by flow interaction with the fences. As created in Eq. (6), the bulk drag coefficient ( $\bar{C}_d$ ) can be formed for fence samples as:

$$\bar{C}_d = \frac{2g \cdot G_B}{D \cdot N \cdot u_n^2} \quad (7)$$

From here, the links between the  $\bar{C}_d$  and the Reynolds numbers in this study are illustrated in Fig. 5 along with several previous studies [17, 18, 33]. It is noted that the porous velocity ( $u_n$ , m/s) will be used from Eq. (5) to describe the flow states inside the sample (via porous Reynolds number,  $Re_n$ ). As can be seen, the  $\bar{C}_d$  and  $Re_n$  for all presented cases indicates a similar trend is indicated, a decrease of the drag with an increase of the Reynolds number. The highest value of  $\bar{C}_d$  appears in early stage of flow (low velocity), in which laminar flows are dominant. For both cases in this study, the  $Re_n$  are larger than the previous studies due to the larger cylinder diameter (0.02 m) and higher density. Hence, the laminar stages occur at around 500 to 1000 of  $Re_n$  in this study while it is around 50 to 200 in previous studies.

It is noted that the higher drag forces at low flow velocity are due to the larger opposite forces around the cylinders and gaps between cylinders [28, 33]. This makes a remarkably high value of  $\bar{C}_d$  at a low flow velocity for both cases (Fig. 5). Hence, the  $\bar{C}_d$  reduces and then finds a stable value at higher  $Re_n$  values. In Fig. 5, the  $\bar{C}_d$  reaches around 2.0 at a significantly large  $Re_n$  ( $> 2000$ ) for the lower density (607 cylinders/m<sup>2</sup>), and it is even higher for a more dense sample (1209 cylinders/m<sup>2</sup>). Additionally, the  $\bar{C}_d$  of case 2 could even be reduced to a lower level at even more turbulent ( $Re_n > 10^5$ ). The more turbulent, the more stable the value of  $\bar{C}_d$ .

From the results in Fig. 5, the links between  $\bar{C}_d$  and  $Re_n$  in this study can be formed as the trending equations and presented with previous studies in Table 3.

In this study, the test samples inherit the real scale of the brushwood fence's inner part, showing a diameter of 0.02 m. The results reflect the flow mechanisms of the scale that appears in the field. However, the reflection of the completely inhomogeneous arrangement of the real brushwood is tragically acknowledged without fully understanding. Therefore, it is necessary to control several parameters, including diameter, density (and porosity), to achieve the desired drag coefficients for further studies.

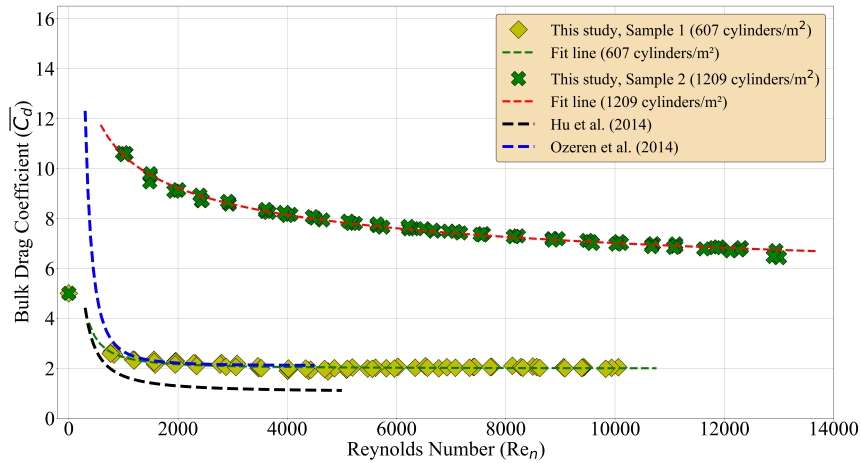


Figure 5. Bulk drag coefficient and Reynolds number in this study in comparison with previous studies

Table 3. Formulas of  $\bar{C}_d$  and  $Re_n$

Study	Formulas	Best fits ( $R^2$ )	Sample descriptions
This study	$\bar{C}_d = 1.98 + \left(\frac{572}{Re_n}\right)^{1.39}$	0.84	Materials: Bamboo cylinders Arrangement: Staggered Diameter: 0.02 m Density: 607 cylinders/m <sup>2</sup> Flow: Steady flow
This study	$\bar{C}_d = 3.26 + \left(\frac{10^6}{Re_n}\right)^{0.29}$	0.99	Materials: Bamboo cylinders Arrangement: Staggered Diameter: 0.02 m Density: 1209 cylinders/m <sup>2</sup> Flow: Steady flow
Hu et al. [18]	$\bar{C}_d = 1.04 + \left(\frac{730}{Re_n}\right)^{1.37}$	0.89	Materials: stiff wooden cylinders Arrangement: Staggered Flow: Wave-flow
Ozeren et al. [17]	$\bar{C}_d = 2.10 + \left(\frac{793}{Re_n}\right)^{2.39}$	0.72	Materials: stiff wooden cylinders Arrangement: Staggered Flow: Wave-flow

#### 4. Conclusions

In this study, the bulk drag coefficient of brushwood fences, nature-based breakwater, is assessed by measuring the hydraulic gradient over the sample width and under steady flow discharge. The tested samples used in the experiments are bamboo cylinders with a diameter of 0.02 m, arranged in a staggered configuration at two different densities: 607 and 1209 cylinders per square meter. Hydraulic gradient measurements were used to calculate the drag force across the sample thickness, determining the bulk drag coefficient in relation to the Reynolds number. The results also conclude that the bulk drag coefficient decreases as the Reynolds number increases. In addition, it is found that higher turbulence in the flow leads to a more stable bulk drag coefficient. This study will open the door

for further investigations into flow over permeable structures using digital methodology, supporting future studies on nature-based solutions.

## Acknowledgements

The authors has a great appreciation to Thuyloi University for the PhD program in Hydraulic Engineering.

## References

- [1] Dao, T. H. (2021). [Hydraulic performance of brushwood fences for mangrove replantation in the Mekong Delta](#). PhD thesis, Delft University of Technology, Delft.
- [2] Phan, M. H. (2020). Coastal and seasonal hydrodynamics and morphodynamics of the Mekong Delta. PhD thesis.
- [3] Truong, S. H., Uijttewaal, W. S. J., Stive, M. J. F. (2019). [Exchange processes induced by large horizontal coherent structures in floodplain vegetated channels](#). *Water Resources Research*, 55(3):2014–2032.
- [4] Le, T. X., Vu, H. T. D., Oberle, P., Dang, T. D., Tran, H. B., Le, H. M. (2024). [Hydrodynamics and wave transmission through a hollow triangle breakwater](#). *Estuarine, Coastal and Shelf Science*, 302:108765.
- [5] Dao, T., Stive, M. J. F., Hofland, B., Mai, T. (2018). [Wave Damping due to Wooden Fences along Mangrove Coasts](#). *Journal of Coastal Research*, 34(6):1317–1327.
- [6] Albers, T., von Lieberman, N. (2011). *Current and Erosion Modelling Survey*. Deutsche Gesellschaft für Internationale Zusammenarbeit (GIZ) GmbH Management of Natural Resources in the Coastal Zone of Soc Trang Province.
- [7] Schmitt, K., Albers, T. (2014). [Area coastal protection and the use of bamboo breakwaters in the Mekong Delta](#). In *Coastal Disasters and Climate Change in Vietnam*, Elsevier, 107–132.
- [8] Albers, T., Schmitt, K. (2015). [Dyke design, floodplain restoration and mangrove co-management as parts of an area coastal protection strategy for the mud coasts of the Mekong Delta, Vietnam](#). *Wetlands Ecology and Management*, 23(6):991–1004.
- [9] Albers, T., San, D. C., Schmitt, K. (2013). *Shoreline Management Guidelines: Coastal Protection in the Lower Mekong Delta*. GIZ, Eschborn, Germany.
- [10] Schmitt, K., Albers, T., Pham, T. T., Dinh, S. C. (2013). [Site-specific and integrated adaptation to climate change in the coastal mangrove zone of Soc Trang Province, Viet Nam](#). *Journal of Coastal Conservation*, 17(3):545–558.
- [11] Cuong, C. V., Brown, S., To, H. H., Hockings, M. (2015). [Using Melaleuca fences as soft coastal engineering for mangrove restoration in Kien Giang, Vietnam](#). *Ecological Engineering*, 81:256–265.
- [12] Mai, T., Dao, T., Ngo, A., Mai, C. (2019). [Porosity Effects on Wave Transmission Through a Bamboo Fence](#). In *International Conference on Asian and Pacific Coasts*, Springer Singapore, 1413–1418.
- [13] Mai, C., Ngo, T. T. A., Mai, C. T., Dao, H. T. (2021). [Bamboo Fences as a Nature-Based Measure for Coastal Wetland Protection in Vietnam](#). *Frontiers in Marine Science*, 8:1430.
- [14] Dao, H. T., Hofland, B., Suzuki, T., Stive, M. J. F., Mai, T., Tuan, L. X. (2021). [Numerical and small-scale physical modelling of wave transmission by wooden fences](#). *Journal of Coastal and Hydraulic Structures*, 1.
- [15] Mendez, F. J., Losada, I. J. (2004). [An empirical model to estimate the propagation of random breaking and nonbreaking waves over vegetation fields](#). *Coastal Engineering*, 51(2):103–118.
- [16] Anderson, M. E., Smith, J. M. (2014). [Wave attenuation by flexible, idealised salt marsh vegetation](#). *Coastal Engineering*, 83:82–92.
- [17] Ozeren, Y., Wren, D. G., Wu, W. (2013). [Experimental investigation of wave attenuation through model and live vegetation](#). *Journal of Waterway, Port, Coastal, and Ocean Engineering*, 140(5):04014019.
- [18] Hu, Z., Suzuki, T., Zitman, T., Uittewaal, W., Stive, M. (2014). [Laboratory study on wave dissipation by vegetation in combined current-wave flow](#). *Coastal Engineering*, 88:131–142.
- [19] Yang, W., Li, Q. (2013). [The expanded Morison equation considering inner and outer water hydrodynamic pressure of hollow piers](#). *Ocean Engineering*, 69:79–87.
- [20] Hald, T., Burcharth, H. F. (2001). [An Alternative Stability Equation for Rock Armoured Rubble Mound Breakwaters](#). In *Coastal Engineering 2000*, 1921–1934.



- [21] Tosco, T., Marchisio, D. L., Lince, F., Sethi, R. (2013). [Extension of the Darcy-Forchheimer law for shear-thinning fluids and validation via pore-scale flow simulations](#). *Transport in Porous Media*, 96(1): 1–20.
- [22] Soulaire, C., Quintard, M. (2014). [On the use of a Darcy-Forchheimer like model for a macro-scale description of turbulence in porous media and its application to structured packings](#). *International Journal of Heat and Mass Transfer*, 74:88–100.
- [23] Darcy, H. P. G. (1856). *Les Fontaines publiques de la ville de Dijon. Exposition et application des principes à suivre et des formules à employer dans les questions de distribution d'eau, etc.* V. Dalamont.
- [24] Ergun, S. (1952). Fluid flow through packed columns. *Chemical Engineering Progress*, 48:89–94.
- [25] Ergun, S., Orning, A. A. (1949). [Fluid flow through randomly packed columns and fluidised beds](#). *Industrial & Engineering Chemistry*, 41(6):1179–1184.
- [26] Gent, M. R. A. V. (1993). *Stationary and oscillatory flow through coarse porous media*. Communications on hydraulic and geotechnical engineering, No. 1993-09.
- [27] Gent, M. R. A. V. (1996). [Wave interaction with permeable coastal structures](#). *International Journal of Rock Mechanics and Mining Sciences & Geomechanics Abstracts*, 33(6):A277.
- [28] Jensen, B., Jacobsen, N. G., Christensen, E. D. (2014). [Investigations on the porous media equations and resistance coefficients for coastal structures](#). *Coastal Engineering*, 84:56–72.
- [29] Schewe, G. (1983). [On the force fluctuations acting on a circular cylinder in crossflow from subcritical up to transcritical Reynolds numbers](#). *Journal of Fluid Mechanics*, 133:265–285.
- [30] Nepf, H. M. (1999). [Drag, turbulence, and diffusion in flow through emergent vegetation](#). *Water Resources Research*, 35(2):479–489.
- [31] Tanino, Y., Nepf, H. M. (2008). [Laboratory investigation of mean drag in a random array of rigid, emergent cylinders](#). *Journal of Hydraulic Engineering*, 134(1):34–41.
- [32] Burcharth, H. F., Andersen, O. K. (1995). [On the one-dimensional steady and unsteady porous flow equations](#). *Coastal Engineering*, 24(3–4):233–257.
- [33] Wieselsberger, C. (1922). *New data on the laws of fluid resistance*.